Obrabotka metallov (tekhnologiya, oborudovanie, instrumenty) = Metal Working and Material Science. 2025 vol. 27 no. 2 pp. 238–254
ISSN: 1994-6309 (print) / 2541-819X (online)
DOI: 10.17212/1994-6309-2025-27.2-238-254

NSTU NETI

Obrabotka metallov - Metal Working and Material Science

Journal homepage: http://journals.nstu.ru/obrabotka_metallov

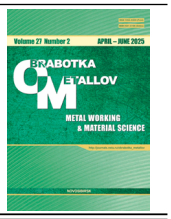

Effect of impact processing on the structure and properties of nickel alloy ZhS6U produced by casting and electron beam additive manufacturing

Andrey Vorontsov [a, *], ***Alexander Panfilov*** [b], ***Alexandra Nikolaeva*** [c], ***Andrey Cheremnov*** [d], ***Evgeny Knyazhev*** [d]

Institute of Strength Physics and Materials Sciences SB RAS, 2/4, pr. Akademicheskii, Tomsk, 634055, Russian Federation

[a] https://orcid.org/0000-0002-4334-7616, vav@ispms.ru; [b] https://orcid.org/0000-0001-8648-0743, alexpl@ispms.tsc.ru;
[c] https://orcid.org/0000-0001-8708-8540, nikolaeva@ispms.tsc.ru; [d] https://orcid.org/0000-0003-2225-8232, amc@ispms.ru;
[e] https://orcid.org/0000-0002-1984-9720, clothoid@ispms.tsc.ru

ARTICLE INFO

Article history:
Received: 06 March 2025
Revised: 27 March 2025
Accepted: 10 April 2025
Available online: 15 June 2025

Keywords:
Impact treatment
Nickel alloy
ZhS6U
Surface hardening
Mechanical processing
Additive manufacturing
EBAM

Funding
The work was carried out within the framework of a grant from the Russian Science Foundation, project No. 23-79-01301.The studies were carried out using equipment from the Center of Collective Use «Nanotech» of the Institute of Strength Physics and Materials Science SB RAS.

ABSTRACT

Introduction. Nickel alloys are widely used in the aerospace industry, but their operational characteristics require improvement through surface modification. A relevant challenge is to conduct a comparative analysis of mechanical impulse processing methods for cast and additively manufactured *ZhS6U* alloy to optimize their properties. ***The purpose*** of this work is to investigate the influence of low-frequency (*LF*) and high-frequency (*HF*) impact processing on the structural-phase state and surface properties of nickel alloy *ZhS6U*, produced by electron beam additive manufacturing (*EBAM*) and casting. The **research methods** include microstructural analysis using optical microscopy, X-ray diffraction analysis of the phase composition, microhardness measurements, and tribological testing via scratch testing of *ZhS6U* alloy samples after various processing modes. **Results and discussion**. It is established that *LF* processing of the cast alloy increases the volume fraction of the strengthening **γ'** phase, while *HF* processing forms an additional Ti_2O phase. The processing of the additive alloy demonstrates more significant changes: micro-strains in the crystal lattice are 1.71…2.18 times higher, micro-stresses in the surface layer are 2.09…2.73 times higher, and the microhardness of the processed surface of the additively manufactured *ZhS6U* alloy is 8…16% higher compared to the cast material. Optimal processing modes are identified to be: 40 seconds for *LF* and 20 minutes for *HF*, providing a minimum friction coefficient of 0.075. **Conclusions**. Mechanical impulse processing effectively hardens the surface of nickel alloy *ZhS6U* fabricated by different methods. The application of the developed approaches is recommended to improve the performance characteristics of parts in the aerospace and mechanical engineering industries. Further research is required on the cyclic stability of modified structures after mechanical impulse processing in various frequency ranges.

For citation: Vorontsov A.V., Panfilov A.O., Nikolaeva A.V., Cheremnov A.V., Knyazhev E.O. Effect of impact processing on the structure and properties of nickel alloy ZhS6U produced by casting and electron beam additive manufacturing. *Obrabotka metallov (tekhnologiya, oborudovanie, instrumenty) = Metal Working and Material Science*, 2025, vol. 27, no. 2, pp. 238–254. DOI: 10.17212/1994-6309-2025-27.2-238-254. (In Russian).

Introduction

Nickel alloys are widely used in aerospace and mechanical engineering at high temperatures due to their combination of high thermal resistance, toughness, and corrosive resistance [1, 2]. Production of these alloys by conventional methods, such as casting and forging, is time-consuming, has limitations in producing complex-shaped pieces, and can lead to high internal stresses and defects [3]. Compared to

*** Corresponding author**
Vorontsov Andrey V., Ph.D. (Engineering), Researcher
Institute of Strength Physics and Materials Sciences SB RAS,
2/4, pr. Akademicheskii,
634055, Tomsk, Russian Federation
Tel.: +7 983 239 3417, **e-mail:** vav@ispms.ru

conventional production methods, additive technologies can eliminate these disadvantages, providing high accuracy and speed in nickel alloy production, and minimize the formation of defects [4, 5] and allow the components to be repaired [6].

The main problem with nickel alloys produced by various methods is the formation of cracks that spread deep into the material over time, contributing to fatigue failure and a reduced product lifespan [7–10]. To minimize fatigue failure of nickel alloys, various methods of surface modification are used, such as laser shock treatment [11, 12], sand blasting [13], shot blasting [14] and electric discharge machining [15, 16].

In [17], the authors investigated the effect of laser shock treatment on the mechanical properties and microstructure of nickel alloy *K403*. Fatigue tests revealed that the formed nanocrystalline layer significantly increases the fatigue life of the alloy under high-frequency cyclic loading, resulting in a 2.44-fold increase in the samples' lifespan compared to the initial state.

In [18], the authors investigated the effect of ultrasonic nanocrystalline surface modification on the reduction of hydrogen embrittlement of *Inconel-625* nickel alloy fabricated by additive manufacturing. Tensile tests showed that after hydrogen saturation, the samples showed an increase in the percentage of elongation of about 6.3 % after surface modification. Grain refinement, as well as formation of residual compression stresses and an increase in dislocation density, which also prevents hydrogen penetration into the material, cause an improvement of mechanical properties.

The issue of surface modification of nickel alloy by mechanical pulse impact treatment remains poorly studied. At the same time, this method is widely used in industry as an effective way to improve the properties of metallic materials by forming a hardened surface layer, reducing embrittlement, and reducing the residual stress level [19, 20].

The ***purpose of this work*** was to compare the influence of mechanical pulse impact treatment on the change in structural-phase state and surface properties of *ZhS6U* nickel alloy obtained by electron-beam additive manufacturing and casting.

To achieve the purpose, it was necessary to solve the following ***tasks***:

– to determine the effect of mechanical pulse impact treatment on the structural-phase state of the surface of *ZhS6U* nickel alloy produced by casting and by the electron-beam additive manufacturing method (*EBAM*);

– to determine the influence of mechanical impulse impact treatment on microhardness and tribological properties of the surface of *ZhS6U* nickel alloy obtained by casting and electron-beam additive manufacturing.

Materials and methods

In this work, the *ZhS6U* nickel alloy (analog of *K465*) was studied (composition is given in Table), which was produced by casting and electron-beam additive manufacturing (*EBAM*) methods. Mechanical pulse impact treatment of the surface of the *ZhS6U* alloy was performed with a tool made of *VT20* titanium alloy, with the area of contact with the surface of the sample being 5×5 mm.

Composition of *ZhS6U* alloy

Fe	C	*Ni*	*Cr*	*Mo*	*W*	*Co*	*Nb*	*Ti*	*Al*	*Others*
≤1	0.13–0.2	Balance	8.0–9.5	1.2–2.4	9.5–11.0	9.0–10.5	0.8–1.2	2.0–2.9	5.1–6.0	≤0.93

Two impact treatment methods were used to process the *ZhS6U* alloy surface. The first method involved treating the surface of the *ZhS6U* alloy samples with a low-frequency (*LF*) fundamental harmonic of 46.6 Hz and an oscillation amplitude of 498 μm. The exposure times for the samples were 10, 20, and 40 s. The second method involved treating the surface of the alloy samples with a high-frequency (*HF*) impact frequency of 21.8 kHz and an oscillation amplitude of 6 nm. The exposure times for these samples were 5, 10, and 20 min.

Before impact treatment, the surface of the samples was prepared by means of abrasive paper, from rough to fine, as well as 1/0 polishing slurry. The roughness of the obtained initial samples was 0.5±0.1 μm.

During impact treatment, a pre-stress of 65 N was applied for all methods, which is attributed to the dynamic loading process. In the case of low-frequency impact treatment, this pre-stress ensures stable contact between the treatment tool and the surface of the material being treated. In the case of small oscillation amplitudes, this pre-stress facilitates energy dissipation in the contact zone between the impact treatment tool and the sample surface, as well as the absorption of impact energy by the sample surface to induce surface deformation.

The structure and roughness of the samples' surface after impact treatment were investigated by optical microscopy using an *Olympus LEXT OLS4100* confocal laser scanning microscope. The optical microscopy method was also used to study the structure of the processed alloys in cross section. For this purpose, each sample after mechanical impulse treatment was prepared in the normal to the surface of treatment cross section by the standard technique for metallographic studies, including sanding on abrasive paper (*SiC*) with grit up to *P2,000*, followed by finishing polishing on 1/0 polishing slurry. Values of microhardness of the treated surface without preliminary preparation were measured on a *Duramin-5* microhardness tester. The phase composition of the treated surfaces of the samples without preliminary preparation was determined using an X-ray diffractometer *DRON-8* with *CuK*α-radiation. The microstresses were analyzed by evaluating the full width at half maximum (*FWHM*) of the X-ray reflex (220). Due to the absence of a reference (unstressed) sample, the *FWHM* value of the original sample at symmetric geometry of imaging was taken as a starting point. The real *FWHM* (**β**) was calculated using Equation 1:

$$\beta = \sqrt{B^2 - b^2}\ , \tag{1}$$

where ***B*** is *FWHM* reflex (220) after deformation processing; ***b*** is *FWHM* of initial sample's reflex (220).

Equation 2 defined the lattice microstrain (**ε**) for each strain value after deformation processing:

$$\varepsilon = \frac{\beta}{4 \cdot tan\Theta}, \tag{2}$$

where Θ is angular position of the analyzed reflex (220).

Tribological tests of treated surfaces without preliminary preparation were carried out by the scratch-testing method on a *Revetest-RST* macro-scratch tester with a diamond indenter at a constant load of 10 N for 3 mm (radius of curvature is 200 μm).

Results and discussion

Fig. 1 shows optical micrographs of the surfaces of *LF*-treated *ZhS6U* alloy samples. The surface roughness of the cast alloy after *LF* impact treatment ranges from 2 to 5 μm (Fig. 1, *a-c*), which is similar to the surface roughness of the additively manufactured alloy (Fig. 1, *d-f*).

Optical images of the surface of cast and additive alloy samples subjected to *HF* impact treatment are presented in Fig. 2. The formation of an additional layer was observed on the surface of all *HF*-treated nickel alloy samples, the morphology of which varies depending on the impact time. The surface roughness of the cast samples after *HF* treatment is about 2 μm (Fig. 2, *a-c*).

The microstructures of cast (Fig. 3, *a*, *c*, *e*) and additive obtained (Fig. 3, *b*, *d*, *f*) *ZhS6U* alloy in cross section after *LF* mechanical pulse treatment are presented in Figure 3. The analysis of metallographic images showed that the extent of plastic deformation increases with both increasing of processing time and depending on the initial condition of the material. Fig. 3, *b*, *d*, *f* shows that *LF* mechanical pulse treatment of the additively manufactured *ZhS6U* alloy results in the formation of a plastically deformed surface layer, characterized by slip bands of varying orientations, as indicated by black lines and red arrows. The alloy structure changes to a depth of ~90 μm with an increase in the processing time up to 40 seconds (Fig. 3, *f*).

The cross-sectional microstructure of the cast (Fig. 4, *a*, *c*, *e*) and additively manufactured (Fig. 4, *b*, *d*, *f*) *ZhS6U* alloy after *HF* mechanical pulse treatment exhibits differences primarily related to the initial material condition. However, optical microscopy of the cross-sections reveals that the additively manufactured

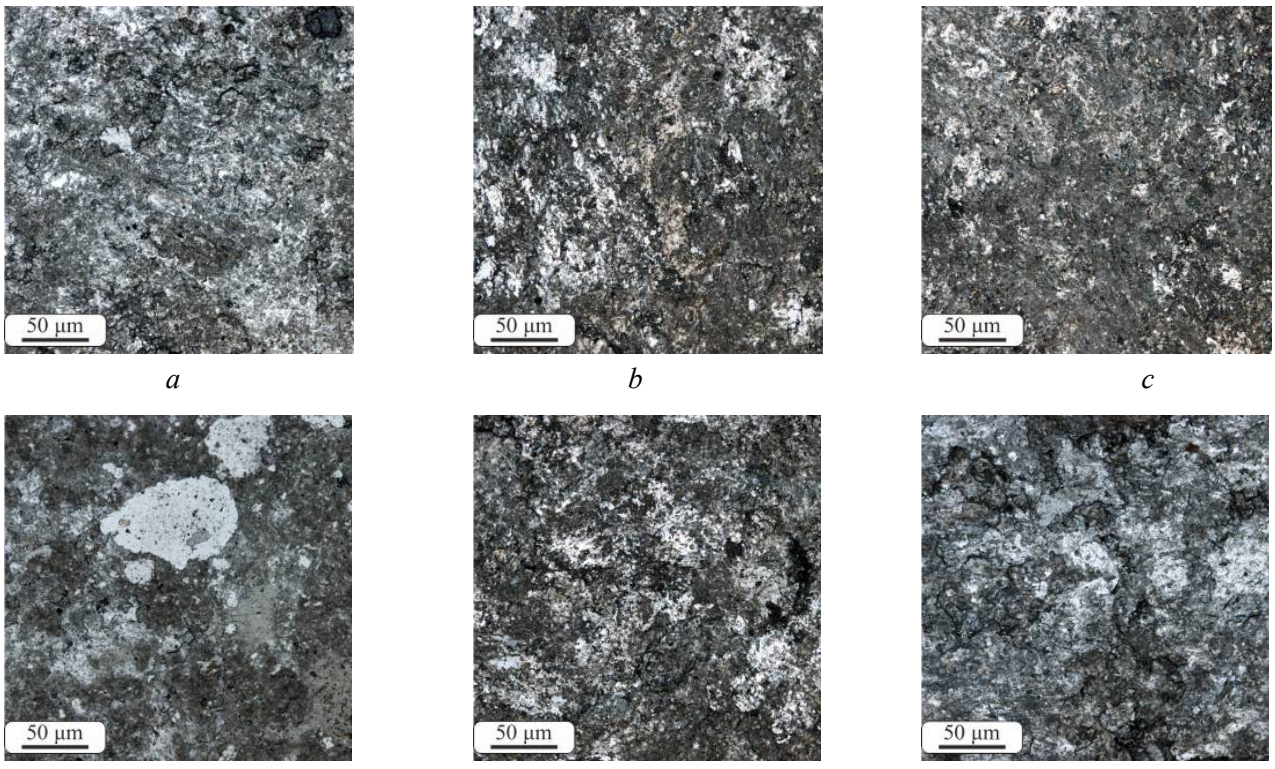

a *b* *c*

d *e* *f*

Fig. 1. Surface microstructure of cast (*a*, *c*, *e*) and additively manufactured (*b*, *d*, *f*) *ZhS6U* alloy after low frequency impact processing for 10 (*a*, *b*), 20 (*c*, *d*) and 40 (*e*, *f*) seconds

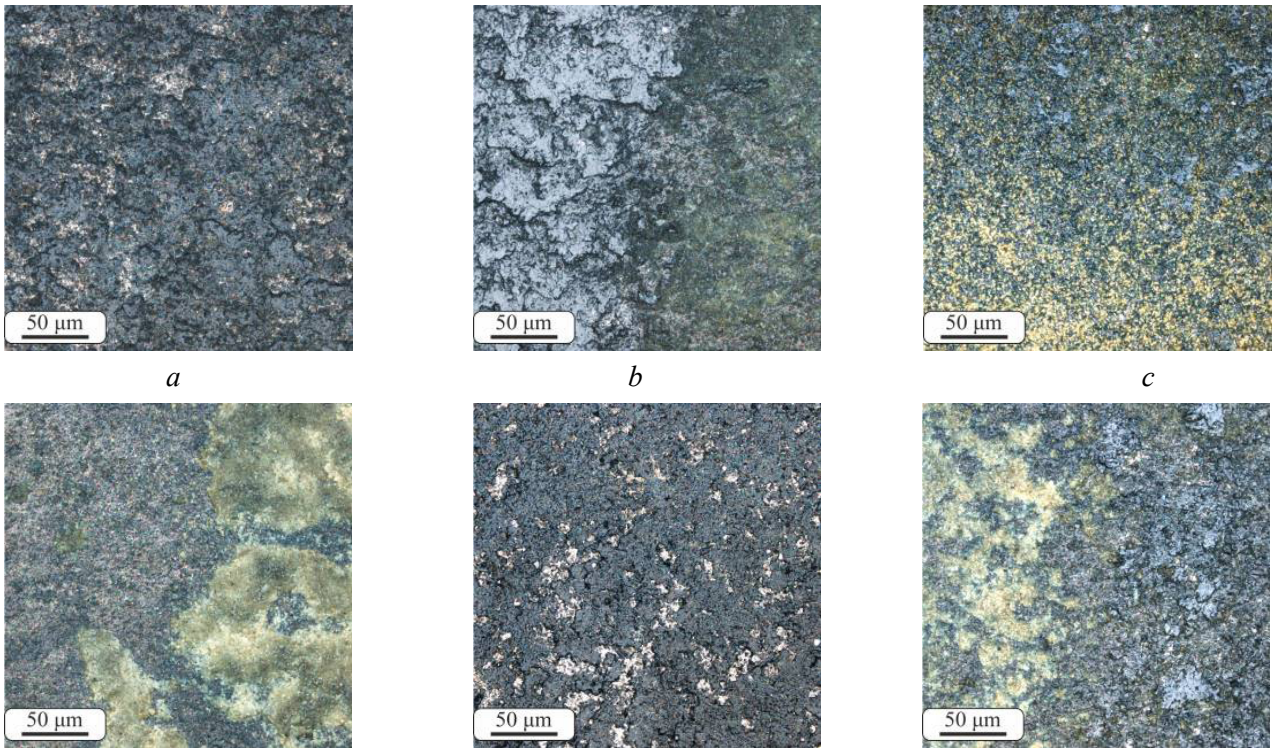

a *b* *c*

d *e* *f*

Fig. 2. Surface microstructure of cast (*a*, *c*, *e*) and additively manufactured (*b*, *d*, *f*) *ZhS6U* alloy after high frequency impact processing for 5 (*a*, *b*), 10 (*c*, *d*) and 20 (*e*, *f*) minutes

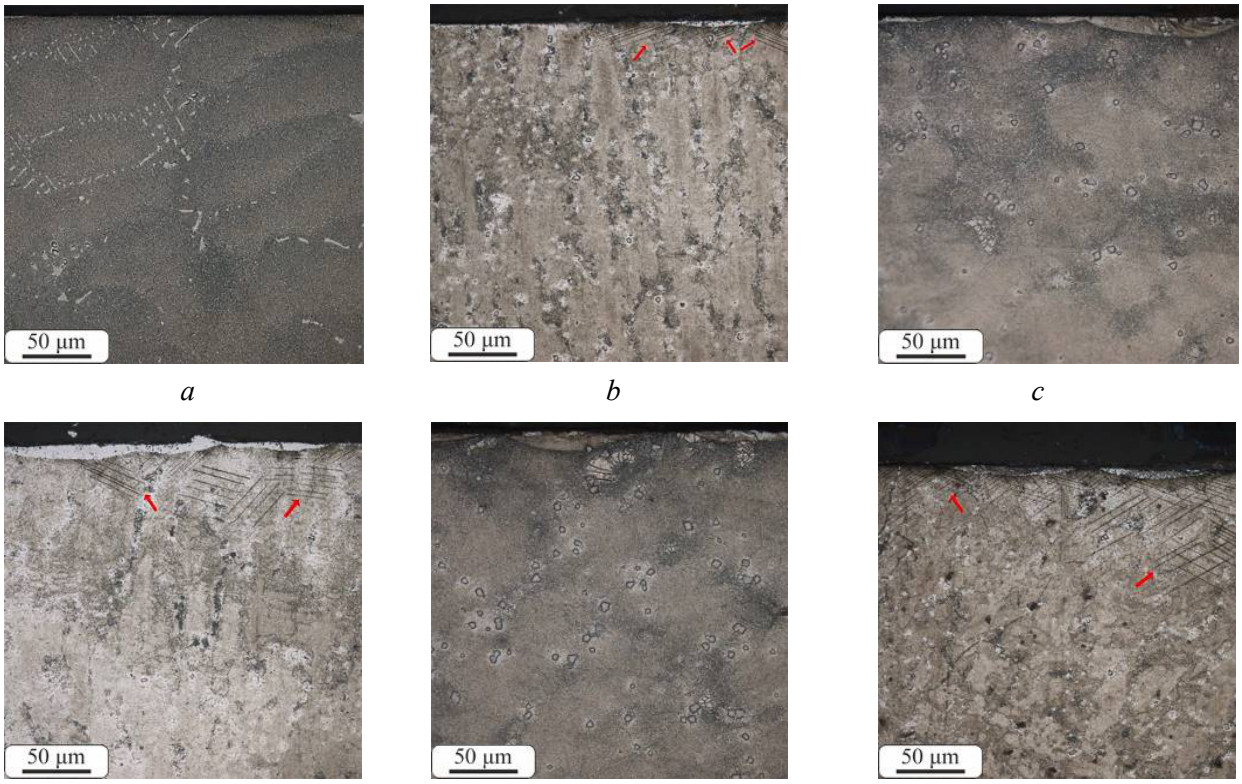

a *b* *c*

d *e* *f*

Fig. 3. Optical microscopy images of *ZhS6U* alloy in cross section: cast (*a*, *c*, *e*) and additively manufactured (*b*, *d*, *f*) after low frequency impact processing for 10 (*a*, *b*), 20 (*c*, *d*) and 40 (*e*, *f*) seconds

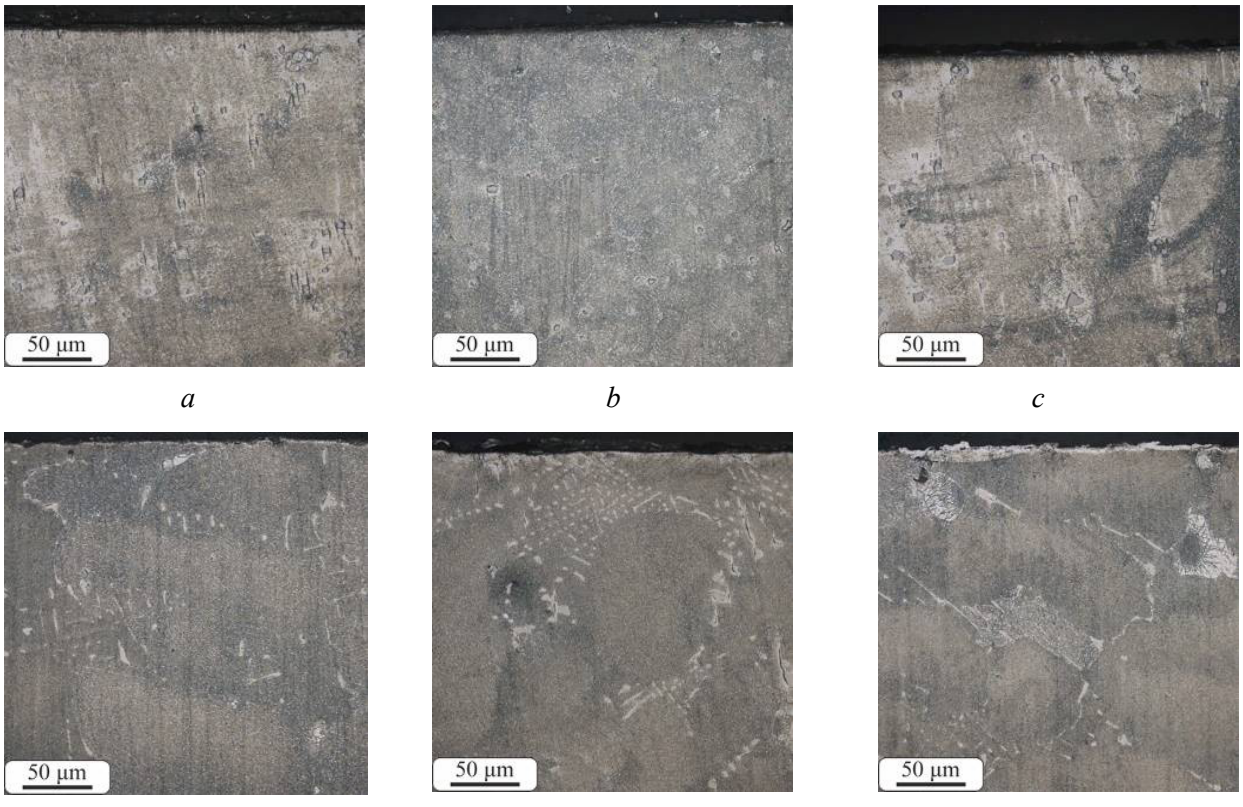

a *b* *c*

d *e* *f*

Fig. 4. Optical microscopy images of *ZhS6U* alloy in cross section: cast (*a*, *c*, *e*) and additively manufactured (*b*, *d*, *f*) after high frequency impact processing for 5 (*a*, *b*), 10 (*c*, *d*) and 20 (*e*, *f*) minutes

samples are more susceptible to deformation with increasing treatment time compared to the cast *ZhS6U* alloy. Structural changes in the cast alloy (Fig. 4, *a*, *c*, *e*) develop more uniformly. Significant grain refinement and an increase in the depth of the modified layer are observed at the maximum treatment time.

X-ray diffraction (*XRD*) analysis of the cast and additively manufactured *ZhS6U* nickel alloy samples after LF impact treatment is presented in Fig. 5. The primary phases, as in the initial material, are *Ni* (γ) and $Ni_3Al(Ti)$ (γ'). An increase in the volume fraction of the γ' phase was observed in the cast samples with increasing *LF* impact treatment time (Fig. 5, *a*).

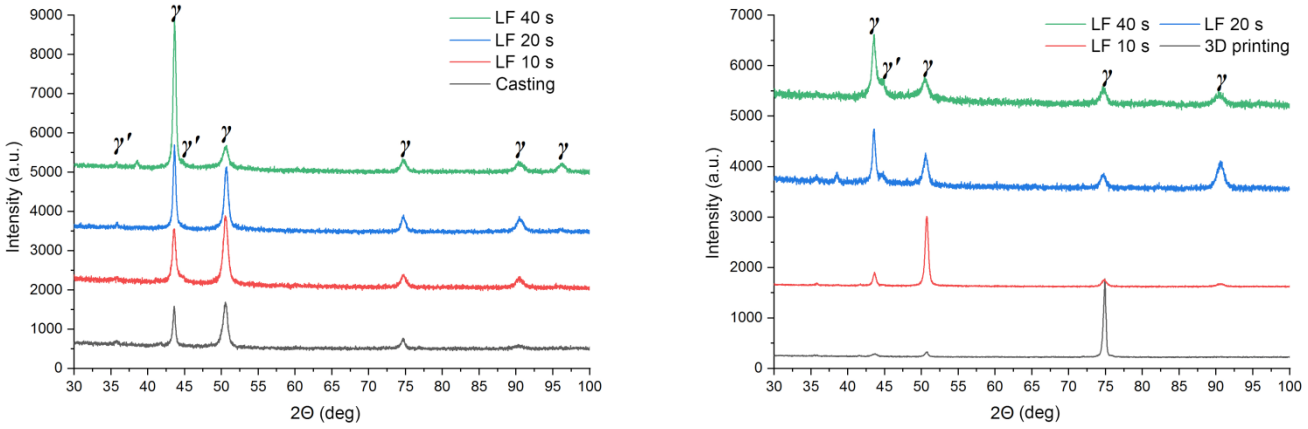

a *b*

Fig. 5. X-ray diffraction profiles of cast (*a*) and additively manufactured (*b*) *ZhS6U* alloy after low frequency impact processing for 10, 20, and 40 seconds

X-ray diffraction (*XRD*) analysis of the cast and additively manufactured *ZhS6U* alloy samples after *HF* impact treatment is presented in Fig. 6. As in the initial material, the primary phases are *Ni* (γ) and $Ni_3Al(Ti)$ (γ'). However, in the case of *HF* impact treatment, a reflection corresponding to the TiO_2 phase is observed (Fig. 6, *a*).

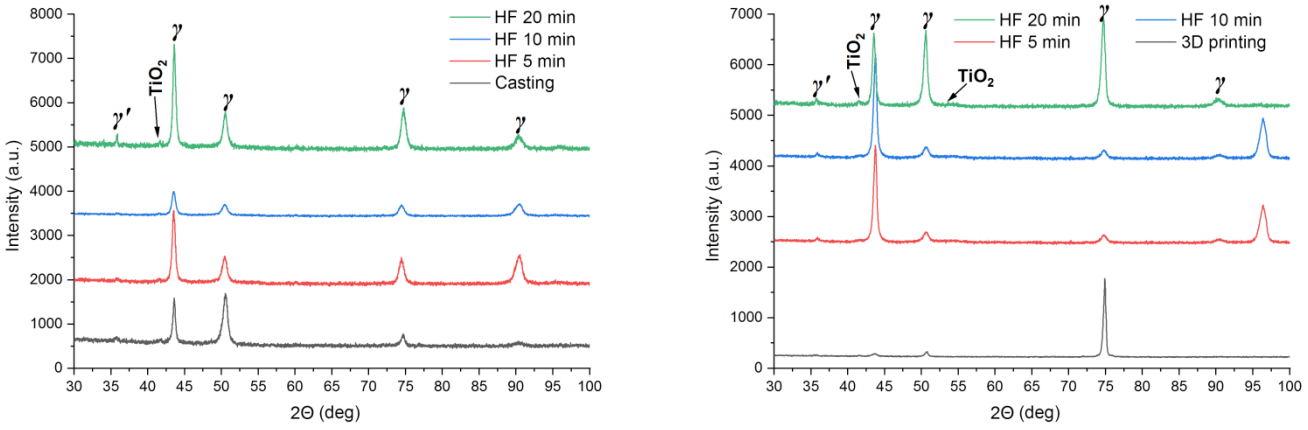

a *b*

Fig. 6. X-ray diffraction profiles of cast (*a*) and additively manufactured (*b*) *ZhS6U* alloy after high frequency impact processing for 5, 10 and 20 minutes

Fig. 7 shows the dependence of microstrain on treatment time for the cast and additively manufactured *ZhS6U* alloy samples after *LF* impact treatment. The cast alloy exhibits a negligible difference in microstrain between the initial material and the sample after 40 seconds of *LF* impact treatment. Specifically, the average lattice strain for the *LF*-treated cast samples is approximately 0.1 %. In contrast, the additively manufactured *ZhS6U* samples show a microstrain of approximately 0.175 % after *LF* impact treatment, increasing to 0.3 % with increasing *LF* treatment time.

Fig. 8 presents the dependence of microstrain on treatment time for the cast and additively manufactured *ZhS6U* alloy samples after *HF* impact treatment. The average lattice microstrain in the cast alloy samples

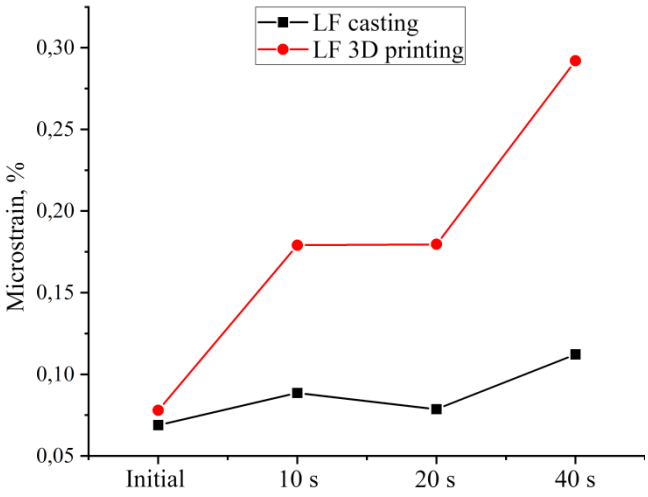

Fig. 7. Micro-strain as a function of processing time for cast and additively manufactured *ZhS6U* alloy samples after low frequency impact processing

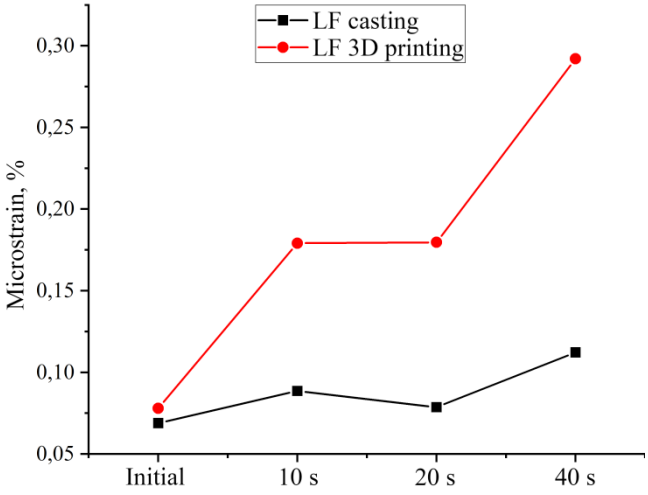

Fig. 8. Micro-strain as a function of processing time for cast and additively manufactured *ZhS6U* alloy samples after high frequency impact processing

was 0.09 % and 0.1 % after 5 and 10 minutes of HF impact treatment, respectively, increasing to 0.11 % with a 20-minute HF treatment time. For the additively manufactured alloy samples, the average lattice strain after 5 and 10 minutes of *HF* impact treatment was 0.2 %, increasing to 0.24 % after 20 minutes of treatment.

Fig. 9 presents the dependence of microstress on treatment time at low frequencies for the cast and additively manufactured *ZhS6U* alloy samples. The curves indicate similar microstress values for both materials in the initial condition. After *LF* impact treatment, the microstress in the cast *ZhS6U* samples was approximately 160 MPa, increasing to 220 MPa with increasing treatment time. Therefore, *LF* impact treatment induces the development of second-order stresses compared to the initial state (~140 MPa) of the cast nickel alloy. In the *ZhS6U* samples obtained by *EBAM*, the microstress after *LF* impact treatment was approximately 300 MPa, increasing to 600 MPa with an increase in treatment time to 40 seconds. Thus, *LF* impact treatment of the *EBAM*- obtained alloy also leads to the development of second-order stresses to a greater extent compared to the initial state (~160 MPa) of the alloy.

Fig. 10 presents the dependence of microstress on treatment time at high frequencies for the cast and additively manufactured *ZhS6U* alloy samples. Similar to the *LF* treatment (Fig. 9), the microstress–treatment time relationship during *HF* treatment reveals a significant difference between the cast and additively manufactured nickel alloys. Specifically, in the cast nickel alloy samples after *HF* impact treatment, the lattice microstress was approximately 185 MPa, increasing smoothly to 230 MPa with increasing treatment time. For the additively manufactured nickel alloy samples after *HF* impact treatment, the lattice microstress increased to 410 MPa, and with the treatment time increasing to 20 minutes, the microstress increased by

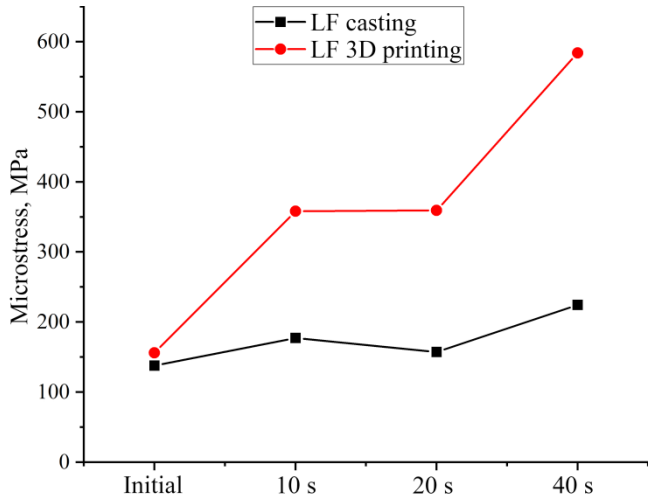

Fig. 9. Micro-stress as a function of processing time for cast and additively manufactured *ZhS6U* alloy samples after low frequency impact processing

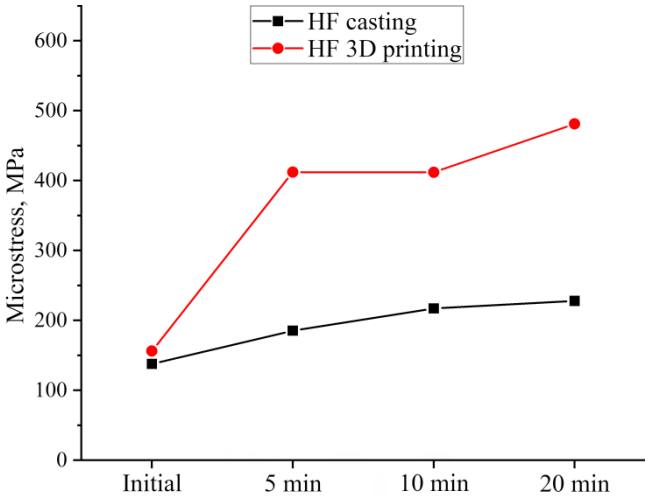

Fig. 10. Micro-stress as a function of processing time for cast and additively manufactured *ZhS6U* alloy samples after high frequency impact processing

70 MPa to a value of 480 MPa. Thus, *HF* impact treatment induces the development of second-order stresses in both alloys compared to their initial states.

The results of microstress evaluation show the similarity of dependences observed at both *LF* (Fig. 9) and *HF* impact treatment (Fig. 10). At the same time, it can be noted that the dependence of the microstress value at *HF* processing differs from *LF* by a smoother change of values.

The average microhardness values of the initial cast and additively obtained *ZhS6U* are 430 and 470 HV, respectively (Fig. 11). The impact treatment of the surface of the *ZhS6U* alloy leads to an increase in the microhardness values. In general, at *LF* impact treatment of the nickel alloy surface for 20 seconds, the microhardness values reach 600 HV. When a cast sample is *LF* impacted for 40 seconds, the microhardness drops to 555 HV. The microhardness of additively manufactured *ZhS6U* at *LF* impact surface treatment reaches values of 650 HV at an impact time of 40 seconds due to the severe plastic deformation process that occurs after *LF* impact surface treatment. The increase in the number of deformation bands indicates a high dislocation density, which increases the microhardness (Fig. 3, *f*).

Surface deformation treatment of cast and additively manufactured *ZhS6U* alloy at high frequencies leads to an increase in microhardness, which is related to the development of plastic deformation and changes in the microstructure of the surface layer (Fig. 4, *a-e*, Fig. 12). During *HF* impact treatment of the cast nickel alloy surface, the microhardness values of the samples increase to 580 HV with an impact time of 5 minutes. When the cast sample is subjected to *HF* impact treatment for 10 minutes, the microhardness decreases to 520 HV; however, with 20 minutes of *HF* impact treatment, it increases again – to 575 HV. At the same time, *HF* impact treatment of the surface of the additively manufactured *ZhS6U* alloy leads to an increase in the microhardness value of the material to 670 HV with an impact time of 10 minutes. *HF* impact treatment for 20 minutes leads to a decrease in microhardness, which is likely due to recrystallization.

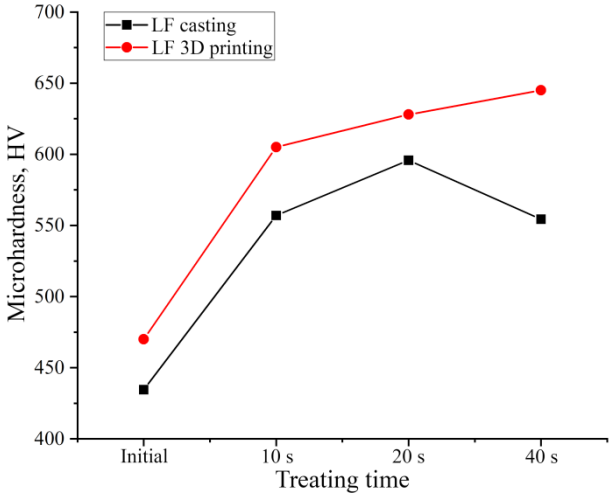

Fig. 11. Microhardness as a function of processing time for cast and additively manufactured *ZhS6U* alloy samples after low frequency impact processing

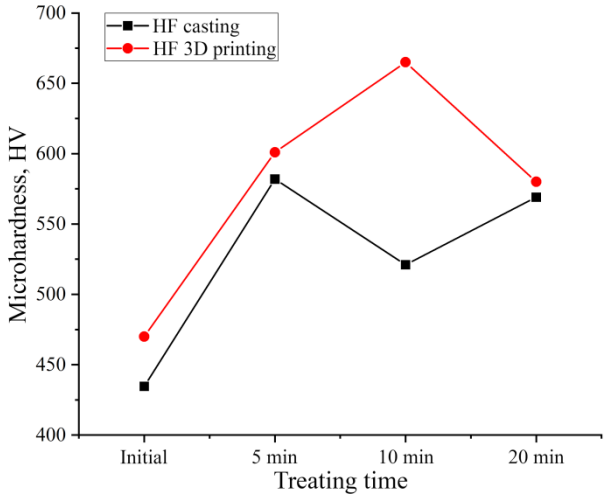

Fig. 12. Microhardness as a function of processing time for cast and additively manufactured *ZhS6U* alloy samples after high frequency impact processing

The results of the scratch test performed after *LF* impact treatment of nickel alloy samples produced by casting and *EBAM* are presented in Fig. 13. The coefficient of friction during scratch testing with a gradually increasing load (from 0.5 to 30 N) of nickel alloy samples after *LF* impact treatment (10–20 seconds) either remains at the level of the initial material (Fig. 13, black line) or increases. At the maximum *LF* treatment duration (40 seconds), the coefficient of friction reaches its minimum value (Fig. 13, *a*, *b*). However, after 40 seconds of treatment, significant scatter in the coefficient of friction is observed depending on the scratch path length during the test, which is caused by surface irregularities.

Scratch testing under a constant load of 20 N also reveals a large scale of the coefficient of friction due to analyzed surface irregularities (Fig. 13, *c, d*). Fig. 13 *e*, *f* shows a final comparison of cast and additively manufactured nickel alloy samples after *LF* impact treatment, based on scratch test results under constant load, in the form of a dependence of averaged friction coefficients. As can be seen on dependences for the cast nickel alloy after *LF* treatment, the coefficient of friction generally increases, with a decrease observed only after the longest treatment time (40 seconds), where the value drops lower than the initial condition (Fig. 13, *e*). Conversely, for the alloy produced by *EBAM*, *LF* impact treatment leads to a decrease compared to the initial condition more than two times – from 0.19 to 0.075.

The results of the scratch test performed after *HF* impact treatment of nickel alloy samples produced by casting and *EBAM* are presented in Fig. 14. The coefficient of friction under a gradually increasing load (0.5 to 30 N) of cast alloy samples after *HF* impact treatment generally remains at the level of the initial material (Fig. 14, black line) or increases, like for the additive sample after 10 minutes of *HF* treatment.

When scratch testing samples after *HF* impact with a constant load of 20 N, a large spread of friction coefficient values is observed (Fig. 14, *c*, *d*), caused by surface roughness after treatment. Fig. 14 *e*, *f* show

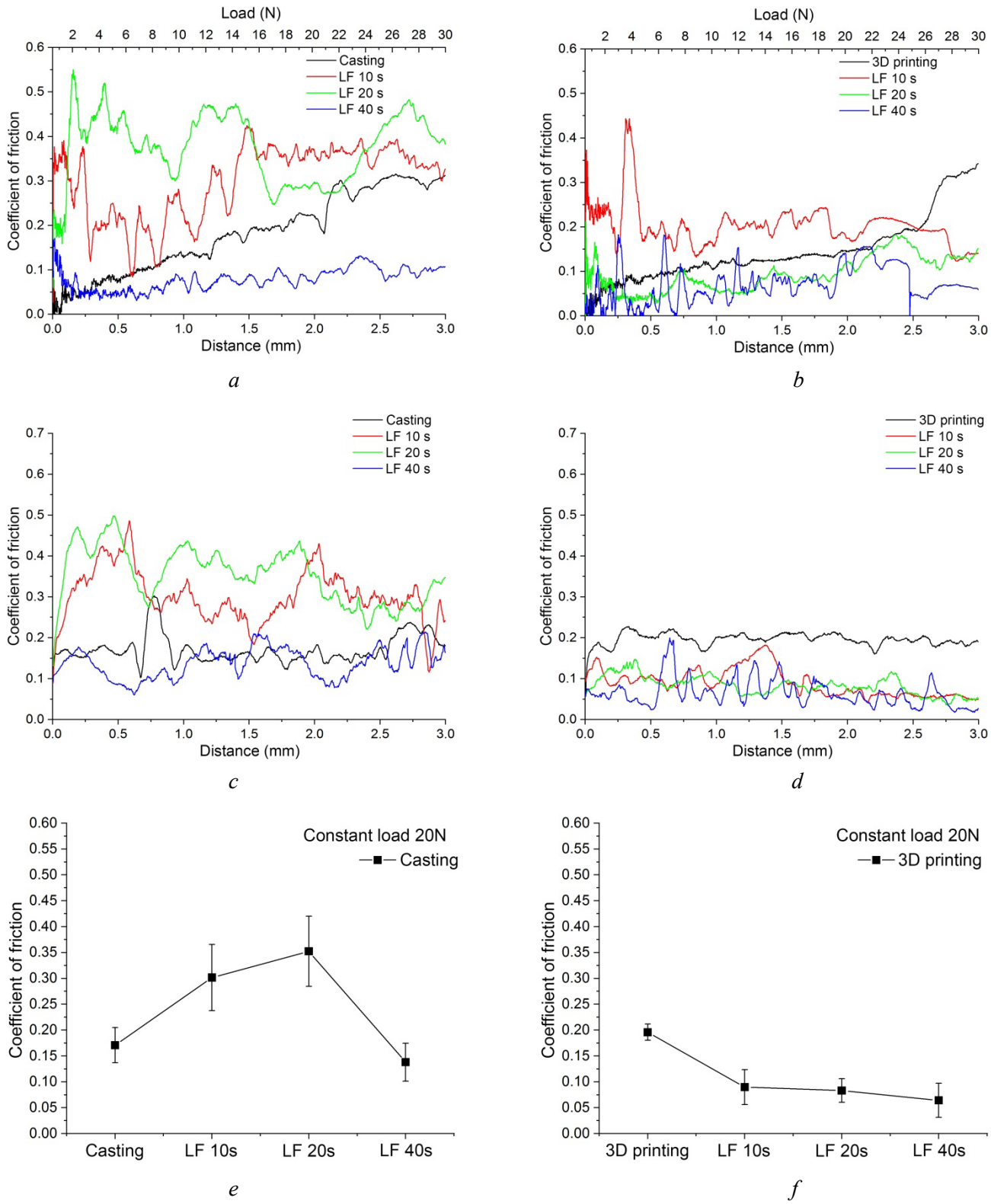

Fig. 13. Scratch test results under varying load (0.5 to 30 N) (*a*, *b*) and constant load (20 N) (*c*, *d*) for cast (*a*, *c*, *e*) and additively manufactured (*b*, *d*, *f*) *ZhS6U* alloy samples after low frequency impact processing, and mean of coefficient of friction of deformed surface under constant load 20 N (*e*, *f*)

a final comparison of the analyzed samples after *HF* impact treatment, based on constant loading scratch testing and presented as the average coefficient of friction dependences. The dependences show that *HF* impact treatment of cast nickel alloy leads to an increase in the tendency of the coefficient of friction, with a decrease observed only at the maximum treatment time (40 seconds), where the coefficient drops to 0.125 compared to 0.17 in the initial condition (Fig. 14, *e*). After *HF* impact treatment of the *EBAM* sample,

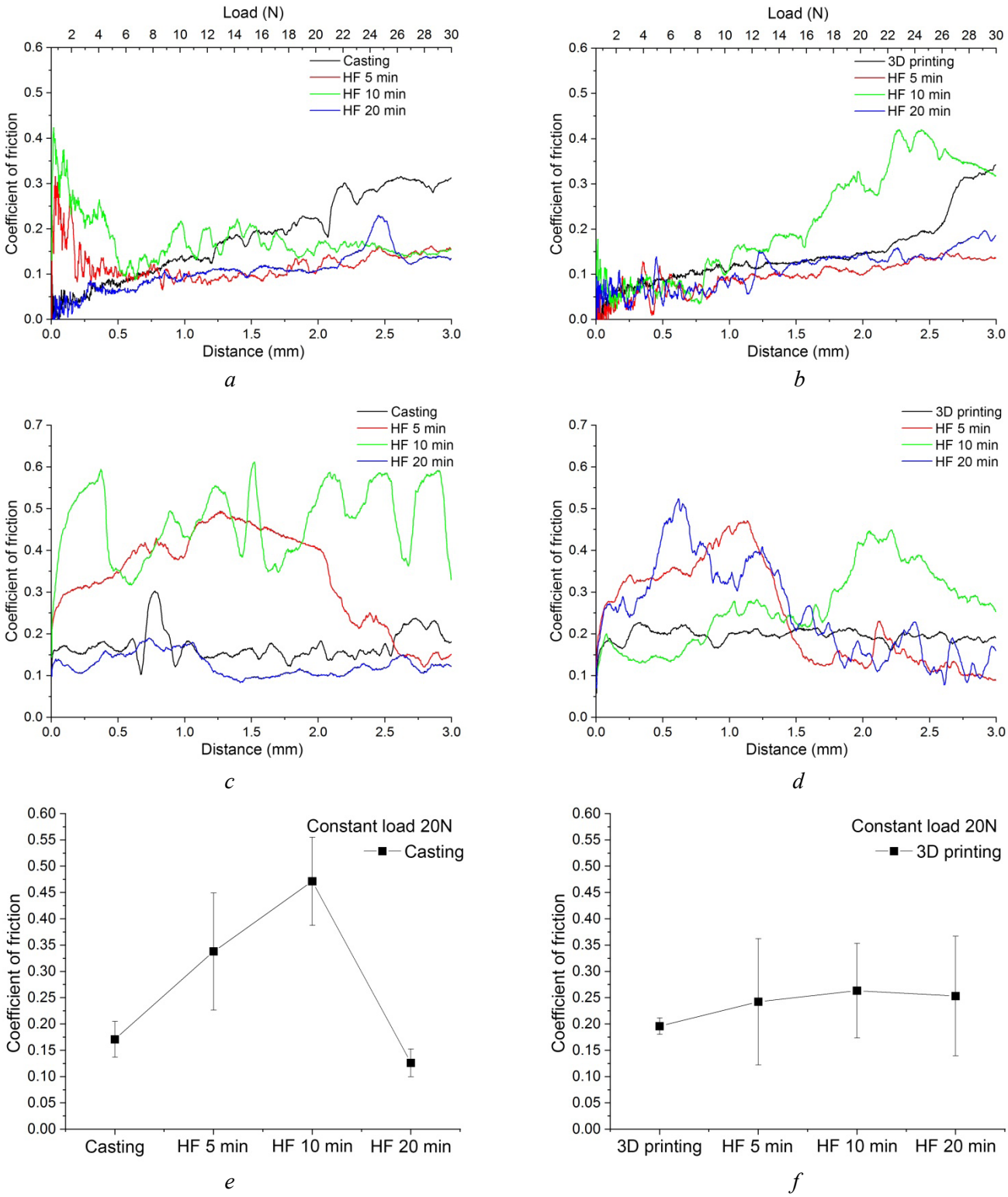

Fig. 14. Scratch test results under varying load (0.5 to 30 N) (*a*, *b*) and constant load (20 N) (*c*, *d*) for cast (*a*, *c*, *e*) and additively manufactured (*b*, *d*, *f*) *ZhS6U* alloy samples after high frequency impact processing, and mean of coefficient of friction of deformed surface under constant load 20 N (*e*, *f*)

increasing duration initially results in a gradual increase in friction. After 20 minutes of treatment, the coefficient of friction is slightly lower than that of the 10-minute sample. With an increase in *HF* impact treatment time of the *EBAM* alloy, the coefficient of friction gradually increases. The coefficient of friction after 20 minutes of *HF* treatment is a little less than the one for the sample after 10 minutes of *HF* treatment.

The performed investigations revealed a complex effect of low-frequency (*LF*) and high-frequency (*HF*) impact treatment on the structure-property relationships of cast and additively manufactured *ZhS6U*

nickel alloy. Analysis showed that both treatment methods significantly modify the surface and bulk of the material; however, the nature of the changes depends on both the frequency of the impact and the initial state of the alloy.

During *LF* treatment of the cast alloy, an increase in the volume fraction of the strengthening **γ'** phase (Ni_3Al(*Ti*)) is observed, correlating with an increase in microstrains up to 220 MPa and microstrains up to 0.1 %. For the additively manufactured alloy, a similar treatment induces more pronounced changes: microstresses reach 600 MPa, and strains reach 0.3 %, which is probably related to the initial inhomogeneity of the structure characteristic, typical for additive technologies. *HF* treatment, in contrast, leads to the formation of an additional surface layer containing the TiO_2 phase, which is absent after *LF* treatment. This suggests thermo-activation processes, such as oxidation, that are activated by high-frequency impact.

The mechanical properties of the alloys exhibit a dependence on the treatment method and initial structure. The microhardness of both materials increases after impact treatment; however, the additively manufactured alloy retains its advantage: after *LF* impact treatment, its hardness reaches 650 HV, compared to 555 HV for the cast counterpart, while after *HF* impact treatment, it reaches 670 HV compared to 580 HV. Interestingly, a decrease in hardness is observed with prolonged treatment (40 seconds of *LF* treatment or 20 minutes of *HF* treatment), which may be explained by stress relaxation or partial recrystallization. The additively manufactured alloy also exhibits increased sensitivity to stress accumulation: after *LF* impact treatment, its microstresses are 2–3 times higher than those of the cast material, due to defects typical of additively manufactured production. *HF* impact treatment, in turn, causes a smoother increase in stresses, likely due to the lower intensity of plastic deformation at high frequencies.

The tribological properties of the alloys, assessed using scratch testing, demonstrate mixed trends. For the cast alloy, *LF* treatment reduces the coefficient of friction only at the maximum treatment time (40 seconds), whereas the additively manufactured alloy shows a progressive reduction in friction from 0.19 to 0.075, which may be associated with surface hardening and a reduction in adhesion. *HF* treatment leads to opposite effects: friction decreases in the cast alloy with longer treatment, while temporarily increasing in the additively manufactured alloy, correlating with the formation and instability of the TiO_2 oxide layer. The scatter in the coefficient of friction values, particularly noticeable under a constant load of 20 N, is explained by the surface roughness after impact treatment.

Comparing *LF* and *HF* treatments highlights their key features. *LF* treatment provides intensive strengthening but is accompanied by a significant increase in stresses, particularly critical for the additively manufactured alloy. *HF* treatment, in contrast, promotes the formation of multiphase surface layers involving oxide phases, which potentially improves wear resistance; however, it requires careful selection of treatment time to minimize softening. These differences necessitate an individualized approach to selecting treatment parameters depending on the alloy manufacturing method.

In conclusion, this study confirms that the additively manufactured *ZhS6U* alloy, despite its initially high hardness, requires caution during long *LF* treatment due to its tendency to accumulate stresses. *HF* treatment, in turn, opens up opportunities for controlling the structure of the surface layer, but its effectiveness depends on the stability of the phases formed. For practical application of the results, further research is important, focusing on evaluating the cyclic stability of modified structures and their corrosion resistance under operating conditions.

Conclusion

The structural-phase state of the treated surfaces after low-frequency (*LF*) and high-frequency (*HF*) impact treatment is similar for both alloys. The main phases in both materials, as in the initial state, are *Ni*(**γ**) and Ni_3Al(*T*i) (**γ'**). However, *LF* impact treatment of the cast *ZhS6U* alloy leads to an increase in the volume fraction of the **γ'** phase, while *HF* impact treatment results in the formation of TiO_2 in the alloy. In addition, high-frequency impact treatment of both alloys leads to the formation of an additional layer on the treated surface, the morphology of which depends on the treatment time.

Electron beam additive manufacturing (*EBAM*) alloy samples exhibited higher values of lattice microstrains, microstresses, and surface microhardness compared to the cast alloy samples, regardless of

the treatment frequency and duration. For example, *LF* treatment of the additively manufactured sample results in microstrain values 1.71 times higher, microstress values 2.73 times higher, and microhardness values 1.08 times higher than the cast sample. With *HF* treatment, the lattice microstrain values of the additively manufactured sample are 2.18 times higher than those of the cast sample, the microstress values are 2.09 times higher, and the microhardness values are 1.16 times higher.

The values of the coefficient of friction depend on the treatment time. With both low- and high-frequency impact treatment, the coefficient of friction of the cast *ZhS6U* increased up to the third control point (20 seconds for *LF* treatment, 20 min for *HF* treatment), after which it sharply decreased, reaching values lower than those of the initial material. *LF* treatment of *ZhS6U* obtained by *EBAM* led to a gradual decrease in the coefficient of friction, while *HF* impact treatment led to a gradual increase in the coefficient of friction with a slight decrease at the fourth control point (20 minutes).

Thus, the treatments have a significant influence on the phase composition, mechanical properties, and tribological characteristics of the alloys. The additive material, in contrast to the cast, exhibits increased sensitivity to external influences, which is expressed in higher microstrains, stresses, and a unique friction response. These characteristics may be related to the initial microstructure formed by the additive manufacturing method.

This work demonstrates the possibility of effectively strengthening nickel-based *ZhS6U* alloy produced by casting and additive manufacturing through mechanical impulse treatment in different frequency ranges. This allows for the formation of a surface layer with improved characteristics: the microhardness increases up to 670 HV, the coefficient of friction decreases to 0.075, and a favorable phase structure is formed with the **γ'**-phase or the formation of an additional TiO_2-phase. At the same time, the additively manufactured samples show greater sensitivity to the treatment, which requires optimization of the parameters for each material type, and the developed approaches can be applied in the aerospace and mechanical engineering industries to improve the performance characteristics of components made from heat-resistant nickel alloys.

References

1. Pollock T.M., Tin S. Nickel-based superalloys for advanced turbine engines: chemistry, microstructure and properties. *Journal of Propulsion and Power*, 2006, vol. 22 (2), pp. 361–374. DOI: 10.2514/1.18239.

2. Semiatin S.L., McClary K.E., Rollett A.D., Roberts C.G., Payton E.J., Zhang F., Gabb T.P. Microstructure evolution during supersolvus heat treatment of a powder metallurgy nickel-base superalloy. *Metallurgical and Materials Transactions A: Physical Metallurgy and Materials Science*, 2012, vol. 43, pp. 1649–1661. DOI: 10.1007/s11661-011-1035-y.

3. Zhang J., Huang T., Liu L., Fu H. Advances in solidification characteristics and typical casting defects in nickel-based single crystal superalloys. *Acta Metallurgica Sinica*, 2015, vol. 51 (10), pp. 1163–1178. DOI: 10.11900/0412.1961.2015.00448.

4. Fortuna S.V., Gurianov D.A., Kalashnikov K.N., Chumaevskii A.V., Mironov Yu.P., Kolubaev E.A. Directional solidification of a nickel-based superalloy product structure fabricated on stainless steel substrate by electron beam additive manufacturing. *Metallurgical and Materials Transactions A: Physical Metallurgy and Materials Science*, 2021, vol. 52, pp. 857–870. DOI: 10.1007/s11661-020-06090-8.

5. Ivanov D., Travyanov A., Petrovskiy P., Cheverikin V., Alekseeva A., Khvan A., Logachev I. Evolution of structure and properties of the nickel-based alloy EP718 after the SLM growth and after different types of heat and mechanical treatment. *Additive Manufacturing*, 2017, vol. 18, pp. 269–275. DOI: 10.1016/j.addma.2017.10.015.

6. Babu S.S., Raghavan N., Raplee J., Foster S.J., Frederick C., Haines M., Dinwiddie R., Kirka M.K., Plotkowski A., Lee Y., Dehoff R.R. Additive manufacturing of nickel superalloys: opportunities for innovation and challenges related to qualification. *Metallurgical and Materials Transactions A: Physical Metallurgy and Materials Science*, 2018, vol. 49, pp. 3764–3780. DOI: 10.1007/s11661-018-4702-4.

7. Kulkarni A., Chettri S., Prabhakaran S., Kalainathan S. Effect of laser shock peening without coating on surface morphology and mechanical properties of Nickel-200. *Mechanics of Materials Science and Engineering*, 2017, vol. 9. DOI: 10.2412/mmse.55.5.304.

8. Carter T.J. Common failures in gas turbine blades. *Engineering Failure Analysis*, 2005, vol. 12, pp. 237–247. DOI: 10.1016/j.engfailanal.2004.07.004.

9. Kim H. Study of the fracture of the last stage blade in an aircraft gas turbine. *Engineering Failure Analysis*, 2009, vol. 16 (7), pp. 2318–2324. DOI: 10.1016/j.engfailanal.2009.03.017.

10. Silveira E., Atxaga G., Irisarri A.M. Failure analysis of two sets of aircraft blades. *Engineering Failure Analysis*, 2010, vol. 17 (3), pp. 641–647. DOI: 10.1016/j.engfailanal.2008.10.015.

11. Karthik D., Swaroop S. Laser shock peening enhanced corrosion properties in a nickel-based Inconel 600 superalloy. *Journal of Alloys and Compounds*, 2017, vol. 694, pp. 1309–1319. DOI: 10.1016/j.jallcom.2016.10.093.

12. Chen L., Sun Y., Li L., Ren X. Microstructural evolution and mechanical properties of selective laser melted nickel-based superalloy after post treatment. *Materials Science and Engineering A*, 2020, vol. 792, p. 139649. DOI: 10.1016/j.msea.2020.139649.

13. Chen M., Shen M., Zhu S., Wang F., Wang X. Effect of sand blasting and glass matrix composite coating on oxidation resistance of a nickel-based superalloy at 1000°C. *Corrosion Science*, 2013, vol. 73, pp. 331–341. DOI: 10.1016/j.corsci.2013.04.022.

14. Ghara T., Paul S., Bandyopadhyay P.P. Effect of grit blasting parameters on surface and near-surface properties of different metal alloys. *Journal of Thermal Spray Technology*, 2021, vol. 30, pp. 251–269. DOI: 10.1007/s11666-020-01127-1.

15. Ji R., Yang Z., Jin H., Liu Y., Wang H., Zheng Q., Cheng W., Cai B., Li X. Surface nanocrystallization and enhanced surface mechanical properties of nickel-based superalloy by coupled electric pulse and ultrasonic treatment. *Surface and Coatings Technology*, 2019, vol. 375, pp. 292–302. DOI: 10.1016/j.surfcoat.2019.07.037.

16. Zhang X., Li H., Shao G., Gao J., Zhan M. "Target effect" of pulsed current on the texture evolution behaviour of Ni-based superalloy during electrically-assisted tension. *Journal of Alloys and Compounds*, 2022, vol. 898, p. 162762. DOI: 10.1016/j.jallcom.2021.162762.

17. Wang C., Shen X.J., An Z.B., Zhou L.C., Chai Y. Effects of laser shock processing on microstructure and mechanical properties of K403 nickel-alloy. *Materials Design*, 2016, vol. 89, pp. 582–588. DOI: 10.1016/j.matdes.2015.10.022.

18. Baek S.H., He S., Jang M.S., Back D.H., Jeong D.W., Park S.H. Ultrasonic nanocrystal surface modification effect on reduction of hydrogen embrittlement in Inconel-625 parts fabricated via additive manufacturing process. *Journal of Manufacturing Processes*, 2023, vol. 108, pp. 685–695. DOI: 10.1016/j.jmapro.2023.11.024.

19. Vorontsov A.V., Utyaganova V.R., Zykova A.P. Vliyanie udarnoi obrabotki v raznykh chastotnykh diapazonakh na evolyutsiyu strukturno-fazovogo sostoyaniya poverkhnosti perlitnoi stali [Influence of shock treatment in different frequency ranges on the evolution of structure-phase state of perlite steel surface]. *Izvestiya vysshikh uchebnykh zavedenii. Fizika = Russian Physics Journal*, 2024, vol. 67, iss. 6, pp. 32–38. DOI: 10.17223/00213411/67/6/5. (In Russian).

20. Liu Y., Wang L., Liu H., Zhang B., Zhao G. Effect of electropulsing treatment on corrosion behavior of nickel base corrosion-resistant alloy. *Transactions of Nonferrous Metals Society of China*, 2011, vol. 21 (9), pp. 1970–1975. DOI: 10.1016/s1003-6326(11)60958-8.

Conflicts of Interest

The authors declare no conflict of interest.